Detection of Small Bowel Polyps and Ulcers in Wireless Capsule Endoscopy Videos

Alexandros Karargyris* and Nikolaos Bourbakis, *Fellow, IEEE*

***Abstract*—Over the last decade, wireless capsule endoscopy (WCE) technology has become a very useful tool for diagnosing diseases within the human digestive tract. Physicians using WCE can examine the digestive tract in a minimally invasive way searching for pathological abnormalities such as bleeding, polyps, ulcers, and Crohn's disease. To improve effectiveness of WCE, researchers have developed software methods to automatically detect these diseases at a high rate of success. This paper proposes a novel synergistic methodology for automatically discovering polyps (protrusions) and perforated ulcers in WCE video frames. Finally, results of the methodology are given and statistical comparisons are also presented relevant to other works.**

***Index Terms*—Bleeding, blood based, data mining, endoscopy, medical imaging, polyps, protrusions, small bowel, SUSAN edge detector, ulcers, wireless capsule.**

I. Introduction to Wireless Capsule Endoscopy

AN ESTIMATED 19 million people in the United States suffer from diseases of the small intestine, such as obscure bleeding, Crohn's disease, chronic diarrhea, or cancer [1]. Wireless capsule endoscopy (WCE) is a technology that offers medical doctors (gastroenterologists) the ability to view the interior of the small intestine with a noninvasive procedure.

WCE was invented by a group of researchers in Baltimore in 1989, and later introduced by Given Imaging Ltd., Yoqneam, Israel, as a commercial tool. Given Imaging Ltd. has developed a swallowable wireless capsule PillCam SB2 (see Fig. 1) that has been the only available product on the market since 2002. A competitor, Olympus Corporation, has been selling the EndoCapsule (see Fig. 2)in Europe since 2005, and received Food and Drug Administration approval in September 2007. In general terms, the operational differences between the two products are minor.

At one end of the PillCam capsule, there is a miniaturized color camera and an optical dome with four white light LEDs.

Fig. 1. Capsule PillCam distributed by Given Imaging Ltd.

Fig. 2. EndoCapsule distributed by Olympus Corporation.

The camera can operate up to 8 h and capture more than 50 000 images, which are transmitted wirelessly to a storage device worn by the patient. After an 8-h procedure, the video feedback is uploaded to a workstation where medical personnel can review and examine the endoscopy images.

As of 2010, the US market is dominated by Given Imaging capsule (PillCam SB). More than 300 000 capsules have been sold since 2001 when it was first introduced. The company provides a software package (RAPID) to view the WCE video, offering a bleeding detector feature based on red color. It provides a position estimator of the capsule inside the digestive tract. Additionally, its multiview feature gives a simultaneous view of two or four consecutive video frames in multiple windows. Finally, a library of reference images (RAPID Atlas) is provided so that the user can have easy access to on-screen case images.

Although the company's software is a useful tool, it still has detection and recognition limitations. In addition, the viewing process of a WCE video is in the range of 1 to 2 h even for experienced gastroenterologists [32]. The need for computer algorithms for automated detection of abnormalities is clear. Thus, researchers are developing methodologies for: 1) the automatic detection of abnormalities such as polyps, bleeding, ulcers [14], and abnormal regions (tumors) and 2) finding the boundaries of the digestive organs.

II. Problem Definition

In this section, we provide useful definitions for the targeted problems (polyps and ulcers) and the methodologies used for their solutions.

A. Polyps

Polyps are growing tissues inside the human body. Although polyps usually appear in the colon, stomach, and urinary bladder,

Manuscript received December 14, 2010; revised March 3, 2011 and April 18, 2011; accepted April 27, 2011. Date of publication May 16, 2011; date of current version September 21, 2011. This work was supported in part by the American Institute of Indian Studies. *Asterisk indicates corresponding author*.

*A. Karargyris is with the National Library of Medicine (NLM) of National Institutes of Health (NIH), Bethesda, MD 20894 USA (e-mail: akarargyris@gmail.com).

N. Bourbakis is with the College of Engineering, Assistive Technologies Research Center, Wright State University, Dayton, OH 45435 USA and also with the American Institute of Indian Studies (AIIS), Dayton, OH 45458 USA (e-mail: nikolaos.bourbakis@wright.edu).

Color versions of one or more of the figures in this paper are available online at http://ieeexplore.ieee.org.

Digital Object Identifier 10.1109/TBME.2011.2155064

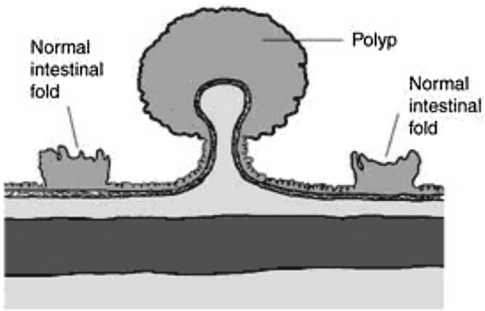

Fig. 3. Graphic representation of a polyp in human colon. National Institute of Diabetes and Digestive and Kidney Diseases, National Institutes of Health.

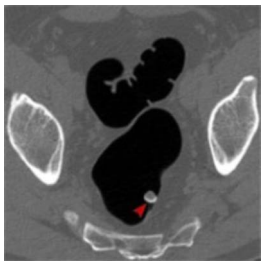

Fig. 4. Polyp pointed with arrow in virtual endoscopy image (*American Journal of Roentgenology*).

they may also appear in the small intestine. A slice of a polyp is shown in Fig. 3.

Polyps can either be malignant or nonmalignant. Most polyps are not cancerous. Polyps can be due to excessive proliferation of tissue, but still be benign and they can also be the result of protrusions of mucosa due to inflammatory conditions or deep-seated malformations or tumors. Physicians may remove them or test them by performing a biopsy [2]. Sometimes polyps can bleed causing anemia, while if they are bigger than 1 cm they have a greater cancer risk associated with them than polyps under 1 cm, although small-sized polyps can turn to be hazardous.

Before the appearance of the WCE, it was a very difficult for medical doctors to examine the small intestine for small-sized polyps noninvasively. A more invasive procedure has been video gastroscopy, which helps physicians examine the upper gastrointestinal tract (esophagus, stomach, and duodenum).

Although the use of gastroscopy is limited to the upper digestive tract, it allows doctors to perform biopsies and/or even resection of polyps, whereas WCE technology cannot yet do for now. Using WCE physicians can detect protrusions as small as 1 to 2 mm and as large as the lumen of the small intestine which is 2.5 to 3 cm.

Besides WCE and gastroscopy technologies, computed tomography colonography (CTC) or virtual endoscopy is used mainly for detecting polyps in the colon noninvasively [33]. Due to the nature of the virtual endoscopy technology, 3-D reconstruction of the colon is feasible. In Fig. 4(a), slice of the colon captured by CTC is presented.

One can see the resemblance between Figs. 3 and 4. In CTC, polyps can be relatively easily identified since they protrude into the colon lumen (see the black color in Fig. 4). Although

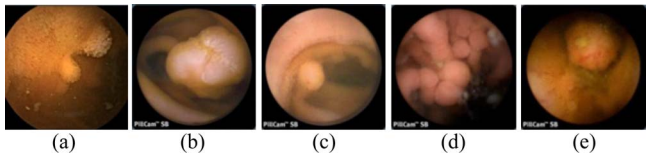

Fig. 5. Polyps in WCE video (Given Imaging EndoCapsule).

CTC is very promising for cancer detection in the colon, this is not the case for the small bowel. Due to limitations of this technology, CTC is not capable of identifying polyps smaller than 1 cm in diameter making it almost pointless to use in the small intestine. Additionally, radiation exposure is a downside of virtual endoscopy.

On the other hand, WCE is the least invasive and least harmful ensdoscopy technology with few side effects. A major side effect is the possibility of having the capsule immobilized inside the digestive tract. In this case, a surgery has to take place to remove the capsule. However, this is very rare. Although WCE offers an inside view of the digestive tract, polyps have great shape irregularity, as it can be seen from the five cases in Fig. 5.

Due the variety in shape, colour, texture, and size of polyps in WCE videos, detection is a difficult task [34]. Consulting with our collaborating doctors, we found out that polyps appear elliptical [see Fig. 3(b) and (e)], round [see Fig. 3(c) and (d)], semicircular [see Fig. 3(a)], and in different sizes [see Fig. 3(a) and (b)]. Although human perception makes it easy to identify polyps, computers algorithms must be sophisticated for automatic detection of polyps in WCE.

Some research has been focused entirely on automatic detection of polyps in WCE videos. In [3], the authors use the discrete wavelet frame transform to extract texture features (color wavelet covariance). In [4], the authors propose a simple methodology that uses color and position features to identify polyps.

However, significant research has been done on automatic detection of polyps in CTC. In [5], the researchers use shape index, curvature, and sphericity ratio as geometric features for polyp candidates. In [6]– [8], the authors use curvature information to extract regions of high curvature and, therefore, polyp candidates. In [8], the authors propose geometric characteristics of polyp shapes: height, radius, boundary length, and mean intensity.

B. Ulcers

In regard to ulcers, the definition of a peptic ulcer is given as an area where tissue has been destroyed by gastric juices. Gastric juices are produced by the stomach and the intestine to digest the starch, fat, and protein in food. Since the intestine and the stomach also consist of proteins, they are protected by 1) mucous layer, 2) bicarbonate, which neutralizes acid, and 3) prostaglandins, which are hormones to boost bicarbonate and mucus production.

Although most peptic ulcers appear in the stomach (gastric ulcers) and the duodenum (duodenal ulcers) they may also appear in the small bowel.

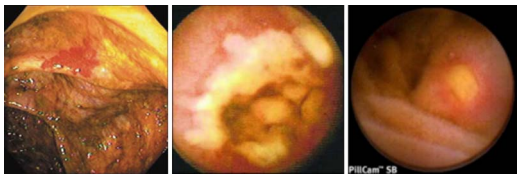

Fig. 6. Three types of ulcers. *Left*: bleeding ulcer. *Middle*: narrowing ulcer. *Right*: perforated ulcer.

Basically, an ulcer can turn into three types of complications: 1) bleeding ulcer; 2) perforated ulcer; and 2) narrowing ulcer. A bleeding ulcer occurs when the ulcer erodes one of the blood vessels. The mortality rate for bleeding peptic ulcers is about 10% [10]. Perforated ulcers [11] appear as a hole in the wall and they are the typical case of peptic ulcers [16]. They can lead to intense abdominal pain. Narrowing ulcers (ulcerated strictures) cause stenosis (stricture) of the intestine and can lead to severe vomiting.

As can be seen in Fig. 6, peptic ulcers vary morphologically. Bleeding ulcer detection can fall into the category of blood-based abnormalities ([12], [13]), whereas narrowing ulcers and perforated ulcers have very different patterns, so that a new detection approach should be made. Our methodology deals with the detection of perforated ulcers, since these are the typical ulcers [16].

III. Synergistic Methodology for Detecting Polyps and Ulcers

From Figs. 5 and 6, it can be seen that both types of abnormalities have similar characteristics regarding:

1) distinct recognizable pattern;
2) geometry.

Characteristic 1) states that small bowel ulcers and polyps can be relatively easily distinguished by experts from the rest of the digestive tract (background).

With characteristic 2), we refer to the shape of each abnormality which is usually round or elliptical.

However, abnormalities have differences that can be contained in:

1) color;
2) crisp distinct edges.

Regarding 3) polyps do not vary in color with the rest of the digestive wall (see Fig. 5) making it hard to use color as a feature for polyp identification. On the other hand, ulcers exhibit color difference (see Fig. 6).

Keeping this useful information in mind, we used a novel methodology that combines mathematical tools and concepts to detect the abnormalities. This detection process is not aiming at replacing experts but helping with reducing the large examination time spent by physicians. Fig. 7 shows the overview of this approach.

In the following paragraphs, each flow of abnormality detection is presented in detail and individually for better understanding.

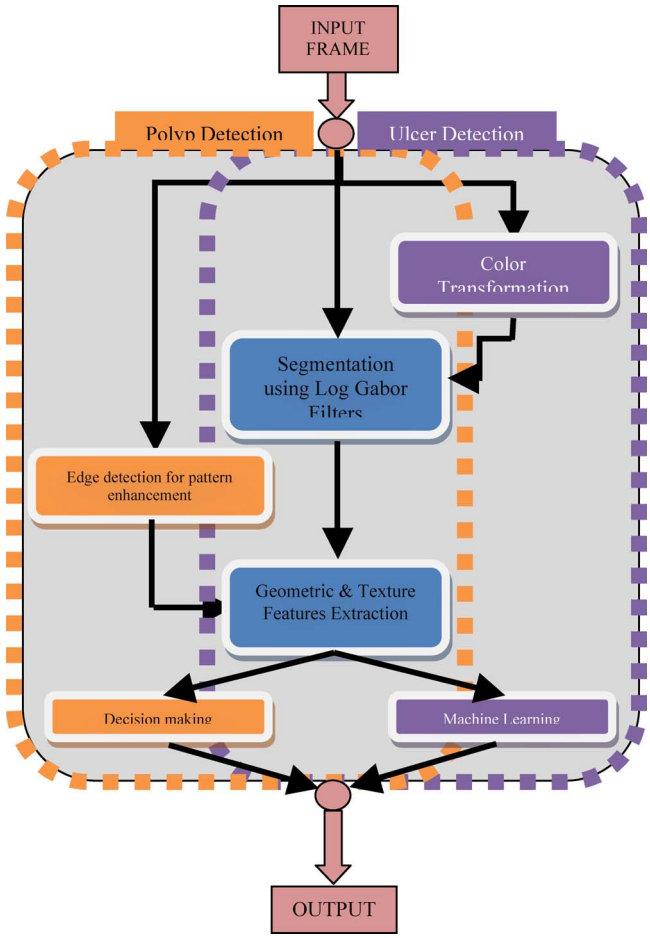

Fig. 7. Overview of synergistic methodology for detecting abnormal patterns such as perforated ulcers and polyps. The flow of the input through each component is shown. Notice that orange is used for components used by the path for polyp identification, purple for ulcer detection and finally blue for detection of both abnormalities.

IV. Detecting Polyps

It is worth mentioning at this point that polyp detection in CTC is a very difficult task and all the previous CTC methodologies are complex and sophisticated in order to reach a high level of accuracy. However difficult this task might be though, suspicious regions can be found on the boundary of the colon lumen (see Fig. 4), whereas in WCE videos polyps can be found anywhere (see Fig. 5). Extraction of polyp candidates in WCE cannot be based on the lumen boundary because in most cases it cannot be seen due to camera's perspective. Therefore, in the case of polyp identification in WCE the most crucial part is the preprocessing step which is the segmentation scheme. The segmentation process must fulfill following two goals.

1) Maintain details of object boundaries.
2) Extract only crisp segments.

However, these two goals cannot be satisfied successfully at the same time using traditional segmentation algorithms based on color or texture values, because these algorithms can either focus on high detail, producing many segments, or focus on crisp segments, losing boundary details. Therefore, we searched for

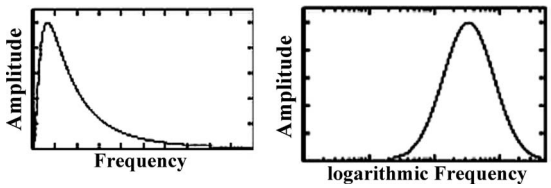

Fig. 8. Log Gabor transfer functions viewed on linear and logarithmic frequency scales.

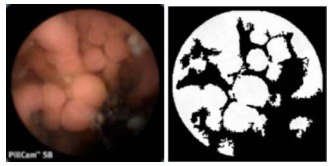

Fig. 9. WCE video frame containing polyps and corresponding Log Gabor filter output.

a different approach of segmentation in order to overcome this issue.

A. Log Gabor Filters and Segmentation

Gabor filters have been widely used in image processing over the last two decades. In [17], Daugmann and in [18] Webster and De Valois showed that Gabor wavelet kernels have many common properties with mammalian visual cortical cells. These properties are orientation selectivity, spatial localization, and spatial frequency characterization. In this sense, Gabor filters offer the best simultaneous localization of spatial and frequency information [19].

However, while Gabor filters are very successful they suffer from bandwidth limitation. To obtain larger spectral information while maintaining maximum spatial localization log Gabor filters have been introduced. Log Gabor filters have a response that is Gaussian when viewed on a logarithmic frequency scale instead of a linear one like Gabor filters. Log Gabor filters can be constructed with arbitrary bandwidth and the bandwidth can be optimized to produce a filter with minimal spatial extent [19]. In [20], Field defines log Gabor filter as follows:

$$G(w) = e^{-[\log(w/w)]^2/2[\log(k/w_o)]^2} \tag{1}$$

where$w$ is the frequency, w_o is the filter's centre frequency, and k/w_o is the filter's bandwidth. The transfer function of the log Gabor function is given in Fig. 8.

Log Gabor functions have two important features:

1) no dc component;
2) an extended tail at the high-frequency end [see Fig. 5(a)].

Feature 1) enables the design of filters in quadrature pairs whereas the transfer function of Gabor filters is the sum of two Gaussians centered at plus and minus the center frequency, thus, resulting in a nonzero dc component, which is undesirable. By removing the dc response we manage to filter out the absolute intensity of the original image and keep meaningful details.

Feature 2) is the most important advantage of log Gabor filters. Field in [20] showed that since log Gabor filters have extended tails on the high frequencies, they are able to encode natural images more efficiently than Gabor functions which suppress higher frequency components and, thus, image details. Finally, Field concludes that log Gabor filter resembles the human visual system that has symmetric cell response on the logarithmic frequency scale.

Keeping in mind the importance of the conclusions that Field has reached, we used log Gabor filter banks to extract crisp regions in WCE video frames. Log Gabor filters behaved successfully as can be seen from the results in Fig. 9.

As can be seen from Fig. 9, log Gabor segmentation process creates meaningful binary regions following at a great extent the human visual system as well pointed by Field.

B. Susan Edge Detector

To further increase the robustness of our methodology, we increased the level of detail of the boundaries by using the promising SUSAN edge detection scheme.

SUSAN stands for Smallest Univalue Segment Assimilating Nucleus and it is described thoroughly in [21]. It follows the traditional method of taking an image and using a predetermined window centered on each pixel in the image it applies a locally acting set of rules to give an edge response. This response is then processed giving as the output a set of edges.

More specifically, a circular mask with Gaussian weighting is placed at each point in the image and for each point the brightness of each pixel within the mask is compared with that of the nucleus (the center point)

$$c(\vec{r}, r\vec{o}) = \begin{cases} 1 & \text{if } |I(\vec{r}) - I(r\vec{o})| \leq t \\ 0 & \text{if } |I(\vec{r}) - I(r\vec{o})| > t \end{cases} \tag{2}$$

where $r\vec{o}$ is the position of the nucleus in the 2-D image, $\vec{r}$ is the position of any other point within the mask, $I(\vec{r})$ is the brightness of the pixel at $\vec{r}$, t is the brightness difference threshold, and c is the output of the comparison. However, using

$$c(\vec{r}, \overrightarrow{r\vec{o}}) = e^{-(I(\vec{r})-I(\overrightarrow{r\vec{o}})/t)^6} \tag{3}$$

gives a smoother version. This allows a pixel's brightness to vary slightly without having too large an effect on c, even if it is near the threshold position. The use of the sixth power can be shown to be the theoretical optimum [21]. Summing the results for each image pixel within the mask gives us

$$n(r\vec{o}) = \sum_{\vec{r}} c(\vec{r}, r\vec{o}). \tag{4}$$

This is the number of pixels inside Univalue Segment Assimilating Nucleus (USAN). Next, the response of the edge is calculated by

$$R(r\vec{o}) = \begin{cases} g - n(r\vec{o}) & \text{if } n(r\vec{o}) < g \\ 0 & \text{otherwise} \end{cases} \tag{5}$$

where g is the geometric threshold of SUSAN algorithm and is set to $3 * \text{nmax} / 4$, nmax is the maximum value which n can take (maximum kernel area) and it is necessary for images that suffer from noise. From the (5), it can be concluded that the smaller

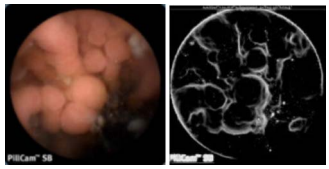

Fig. 10. WCE video frame containing polyps and corresponding SUSAN edge detection output. Brightness_Threshold = 5, USAN_kernel_radius = 5.

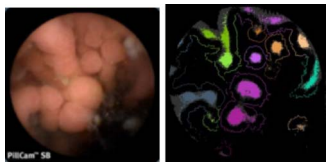

Fig. 11. Clusters of curvature center points with their associated boundary pixels. Each cluster has a different color.

the USAN area, the larger the edge response. In other words, this means that the larger the USAN area, the more probable the area under examination is a surface rather than an edge. In Fig. 10, the output of SUSAN edge detector for a WCE video frame is given.

C. Geometric Features Extraction

Using SUSAN edge detection output and log Gabor output, we manage to produce crisp segments with very detailed boundaries. However, these segments as seen in Fig. 4 are still merged into one big region, and therefore, they need to be turned into single meaningful regions.

To do so, the algorithm runs along the boundaries of the binary image (see Fig. 9) calculating the curvature at each point. For these points that have over a certain curvature, the centers of curvature are found and stored.

The center of curvature (ξ, η) for a boundary pixel (x,y) is given by the following formula:

$$\xi = x - \frac{(x'^2 + y'^2)y'}{x'y'' - x''y'}, \quad \eta = y + \frac{(x'^2 + y'^2)x'}{x'y'' - x''y'}. \tag{6}$$

This results to clouds of curvature center points inside the white segments (see Fig. 9). Still, in order to create single regions a simple two-threshold sequential clustering is applied to the resulting stored points and each curvature center point is assigned to a unique cluster. The clustering result can be seen in Fig. 11.

Starting from each single cluster center a level-set model (see [22]) expands an active contour on the original WCE grayscale frame until it reaches the corresponding boundary pixels of that cluster. In this way, single meaningful regions are extracted.

A region is said to be a polyp candidate if it satisfies two basic rules.

1) During the contour expansion process a great percentage (>85%) of its boundary pixels have been reached.
2) Its eccentricity is above 0.70.

Rule 1) ensures that the extracted region is a real region with clear boundaries while rule 2) makes sure that the shape of the region is an ellipse close to a circle.

V. Detection of Ulcers

A. Color Transformation

There are numerous color spaces but the following stand out: RGB, HSV, CMYK, YPbPr, Luv, Lab.

RGB color space is probably the most well-known color space. It is commonly used in most of the devices for capturing images and it derives from trichromatic theory, which states that there are three types of photoreceptors, sensitive to the red, green, and blue region of the spectrum, approximately. RGB is an additive color space since the final color comes from the addition of its three components: red, green, and blue.

RGB color space suffers from a major disadvantage: in applications with natural images there is a high correlation between its components: about 0.78 for r_{BR} (cross comelation between the B and R channel), 0.98 for r_{RG} and 0.94 for r_{GB} [23]. This was also shown by Ohta *et al.* in [24] where the Karhunen–Loeve transformation of the RGB proved to achieve decorrelation of RGB components.

In 1978, Smith proposed the HSL and HSV color spaces, which are very similar. HSV (Hue, Saturation, Value) color space describes colors the same way human visual system perceives colors. Hue is another word for the dominant frequency of a color mixture. It shows what color we have. Red, blue, and yellow are the primary colors, and when combined in equal amounts they create the secondary hues orange, green, and violet. Saturation is the intensity of a color. Saturated colors are very pure, vivid. Value is the lightness or darkness of a color creating a scale from pure black to pure white.

The RGB-to-HSV transformation is given by

$$h = \begin{cases} 0 & \text{if } \max = \min \\ \left(60^\circ \times \dfrac{g-b}{\max - \min} + 0^\circ\right) \bmod 360^\circ, & \text{if } \max = r \\ 60^\circ \times \dfrac{b-r}{\max - \min} + 120^\circ, & \text{if } \max = g \\ 60^\circ \times \dfrac{r-g}{\max - \min} + 240^\circ, & \text{if } \max = b \end{cases}$$

$$s = \begin{cases} 0, & \text{if } \max = 0 \\ \dfrac{\max - \min}{\max} = 1 - \dfrac{\min}{\max}, & \text{otherwise} \end{cases}$$

$$v = \max \tag{7}$$

where r, g, b are the normalized values [0,1] in RGB color space.

B. Segmentation in RGB Color Space

Besides performing segmentation using log Gabor filters (as described in Section IV-A and shown in Fig. 7) in HSV color space, an additional segmentation process [25] occurs in the original RGB color space to produce crisp ulcer regions.

The segmentation scheme is based on a fuzzy region-growing approach.

First, the input image is smoothed to remove noise. This operation attempts to preserve the location of edges by only smoothing areas where local contrast (within a small neighborhood) is

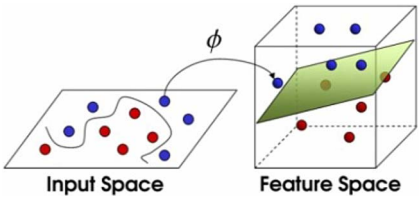

Fig. 12. Mapping of the input space to the feature space. Optimal hyperspace is found for the two-class problem. *Source*: Council of Scientific and Industrial Research.

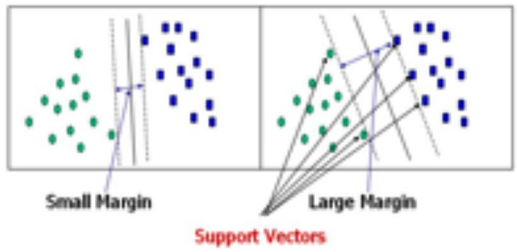

Fig. 13. Margin maximization using SVM. *Source*: DTREG.com.

fairly low. Edge information is used from the smoothed input image. The segmentation algorithm uses edge information and the smoothed image to find segments.

The edge-detection step creates segments that are surrounded by edge pixels or the image boundary. A solid segment is defined as a set of pixels completely surrounded by edge pixels belonging to only one object. To find a solid segment, the image is first scanned for the first nonedge pixel. This pixel is used as a growing seed. In the growing process, a pixel can grow recursively in four directions (left, right, up, and down), and merged with the seed if the growing condition is met. When the growing process ends, if the grown segment is not sufficiently large (i.e., consisting of a threshold quantity of pixels as determined by the image's frequency histogram), the segment is removed. This removal is due to the assumption that the segment found may actually be a part of a larger segment, but was falsely separated because of noise. The weighted average color of the segment is computed, and then the segment is painted with this color.

A distance measure is used to further expand segments. An unassigned pixel can be close (not far) to a neighboring segment in two senses: 1) close in the spatial domain or 2) close in the cluster domain of the color cube. The degree of distance of a pixel to a neighboring segment is defined as a product of these two measures. The closest segment to the pixel is the one having the lowest degree of farness. If this lowest value belongs to the expanding segment, and is lower than a fixed threshold, the pixel is merged with that segment. In that sense, fuzzy logic is used to expand clusters and to generate new clusters. It is also used to merge some pixels with the closest cluster (in color and distance).

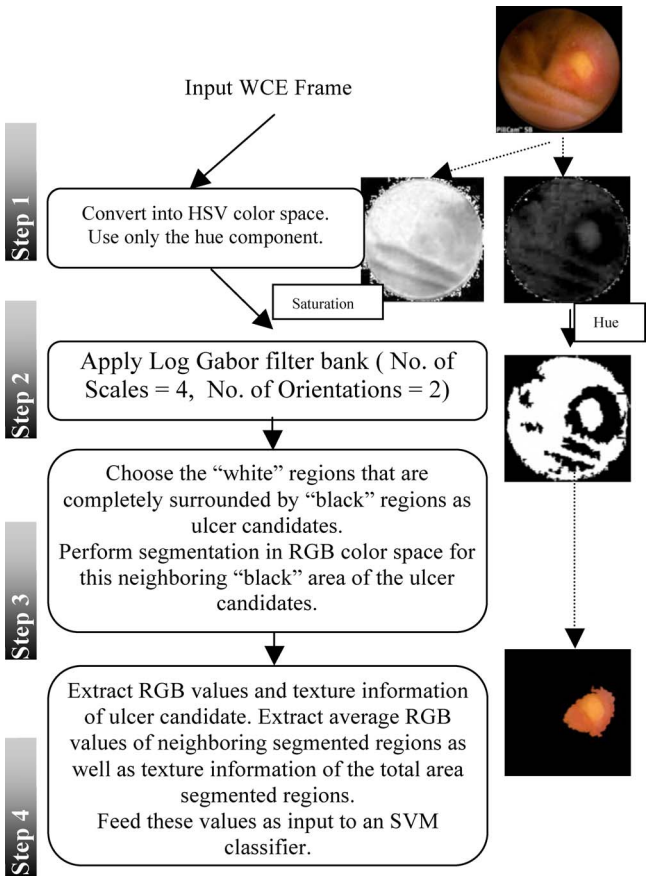

Fig. 14. Flowchart of the ulcer identification methodology.

C. Machine Learning

Support vector machines (SVMs) are supervised learning methods widely used to classify data. The basic concept is that an SVM maps the input data to an n-dimensional space, where it tries to find the optimal hyperplane to separate the datasets [26]. The popularity of SVMs lies on their generalization ability for a wide range of pattern recognition problems. As well put by John Shawe-Taylor and Nello Cristianini: the key features of SVMs are 1) the use of kernels, 2) the absence of local minima, 3) the sparseness of the solution, and 14) the capacity control obtained by optimizing the margin.

The process of SVM is shown in Figs. 12 and 13.

SVM finds the optimal hyperplane that will maximize the margin between the support vectors. Margin is the distance between the dashed lines (see Fig. 13). The vectors that define this margin are called support vectors (see Fig. 13). Therefore, the larger the margin, the smaller the generalization error of the classifier.

All steps of ulcer detection methodology are summarized in Fig. 14.

Fig. 14 demonstrates the algorithmic path for the detection of perforated ulcers in WCE videos. In step 2, one can easily see the importance of hue component to distinguish different colored regions in WCE frames. The saturation channel did not offer a great discriminating power (see step 1 in Fig. 14). Hue makes regions with similar color appear unified, while regions with different colors get separated. Having preprocessed the input frame with the RGB-to-HSV color transformation, log Gabor filtering, as described in Section III-A, creates a robust

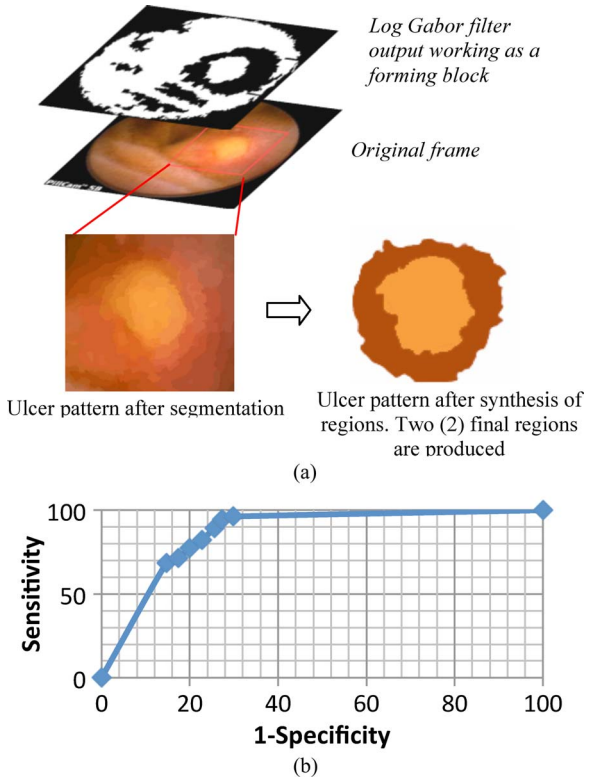

Fig. 15. (a) Extraction of ulcer pattern. (b) ROC for constant boundary pixels percentage experiments.

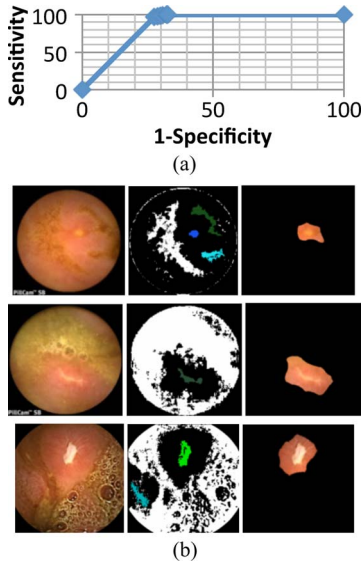

Fig. 16. (a) ROC for constant eccentricity. (b) Three cases of perforated ulcers. *From left to right*: Original Frame; log Gabor output (multiple ulcer candidates are given in different colors); final output.

TABLE I
SENSITIVITY = 100% AND SPECIFICITY = 67.5%

	Polyp Frames	Non polyp frames
Identified	10	13
Not Identified	0	27

binary segmentation of the image. One could argue whether there is a point in performing filtering with log Gabor since a simple hard threshold on hue component could produce the same results. The answer lies exactly on that threshold. A fixed threshold value cannot cope with any given input, whereas log Gabor filtering takes into account the whole input signal while maximizing local frequency and spatial information.

The postlog Gabor processed frame (see step 3) behaves as a forming block for the next step, the main segmentation process in RGB color space: medium-sized regions (shown in white at step 2) are ulcer candidates, so the segmentation scheme extracts the surrounding regions, and synthesizes them [25] to produce only one big crisp surrounding region. By the term "surrounding regions" we experimentally chose regions at a fixed distance (20 pixels since the frame is 380 by 380 pixels) around the white area (ulcer candidate). The procedure is given later.

Having extracted a candidate ulcer pattern (inside region/hole and outside region/rush, see Fig. 15), average RGB values and texture information are calculated on both areas creating a "word" (description) of the ulcer pattern. Texture information consists of traditional statistical texture features described by Haralick *et al*. in [29]. In our case, we used entropy (ENT), contrast (CONT), homogeneity (HOM), and inverse moment (INV). So, we have a word format of 14 values

The pattern word is fed to a fuzzy SVM which is described in [30] for classification of the input pattern.

VI. EXPERIMENTAL RESULTS AND COMPARISONS FOR THE METHODOLOGY

We collaborated with gastroenterologists from Digestive Specialists, Dayton, OH, for collecting polyp cases from various patients. Some of them are shown in Figs. 6 and 7. It is difficult to gather a large number of real cases of abnormalities in WCE videos since patients do not necessarily suffer from an abnormality and if they do, rarely do they carry multiple cases. Additionally, there are restrictions to patients' records. We are planning to extend our dataset in the future since this is a time-consuming and sensitive process.

We ran the algorithm on a 50-frame WCE video containing 10 frames with polyps and 40 normal frames in order to have a rough estimate of the sensitivity (percentage of actual positives) and specificity (cases correctly identified as negatives) of our methodology (see Table I).

Our methodology reached a high percentage of sensitivity because of the criteria selected in Section IV-C eccentricity and boundary pixels percentage. In order to further examine the tuning of these important parameters, we ran two sets of seven different tests. Tables II and III summarize the sensitivity–specificity for various values of the parameters.

We performed an exhaustive search in the scientific community for works related to the detection of polyps in WCE videos because we wanted to compare our methodology with

TABLE II
SENSITIVITY VERSUS SPECIFICITY FOR CONSTANT BOUNDARY PIXELS PERCENTAGE

	Sensitivity	Specificity
Boundary pixels>0.50, E=0.10	68.34	85.34
Boundary pixels>0.50, E=0.20	71.43	82.54
Boundary pixels>0.50, E=0.30	77.43	80.12
Boundary pixels>0.50, E=0.40	82.32	77.31
Boundary pixels>0.50, E=0.50	89.32	74.43
Boundary pixels>0.50, E=0.60	94.68	72.65
Boundary pixels>0.50, E=0.70	96.23	70.23

TABLE III
SENSITIVITY VERSUS SPECIFICITY FOR CONSTANT ECCENTRICITY

	Sensitivity	Specificity
Boundary pixels>0.55, E=0.70	96.75	72.45
Boundary pixels>0.60, E=0.70	97.76	71.23
Boundary pixels>0.65, E=0.70	98.78	70.13
Boundary pixels>0.75, E=0.70	99.23	69.23
Boundary pixels>0.80, E=0.70	99.75	67.72
Boundary pixels>0.85, E=0.70	99.96	67.52
Boundary pixels>0.90, E=0.70	100.00	67.32

TABLE IV
COMPARISON OF POLYP DETECTION METHODOLOGIES

	Sensitivity	Specificity
Texture units	0.9714	0.9428
Color Wavelet Covariance (CWC)	0.9360	0.9930
Discrete Curvelet Transform (DCT)	0.9750	0.9740
Geometric characteristics	0.9675	0.7245

TABLE V
SENSITIVITY = 75.0% AND SPECIFICITY = 73.3%

	Ulcer Frames	Non Ulcer Frames
Identified as ulcers	15	8
Not Identified as ulcers	5	22

TABLE VI
COMPARISON OF ULCER DETECTION OF METHODOLOGIES

	Sensitivity	Specificity
DCT transform [32]	0.8881	0.8419
Log Gabor	0.7500	0.73.30

other methodologies. Unfortunately, we could not find methodologies exclusively focused on the detection of polyps in WCE. However, we were able to find [3], [27], and [28] that try to identify any type of tumors (see Table IV). In all three works, researchers used texture descriptors to describe the texture of the tumors and detection was performed using classifiers.

Morespecifically, in [27] the authors used texture unit transformation (Texture Units-TU) to recognize characteristic relative positions of pixel. In such a way, texture units characterize the local texture information for a given pixel and its neighborhood, and the statistics of all the texture units over the image show the global texture aspects.

In [3], the researchers proposed the use of color wavelet covariance features to describe tumor texture in endoscopic images. In more detail, they perform 2-D discrete wavelet transform on each channel of the image (R, G, and B), then calculate texture measures and finally these are fed to a classifier for detection.

In [28], instead of using a Wavelet transform, the authors use the discrete curvelet transform (DCT). Having extracted the DCT coefficients they produce the textural measure that are fed into traditional multilayer perceptron (MLP) neural network.

For the detection of ulcers, we present three more examples how our methodology behaved with multiple ulcer candidates. We also give some statistical results based on 20 cases of ulcers.

Collecting WCE videos with cases of ulcers is also a hard task.

We managed to run our algorithm on 20 frames with ulcer cases (see Table V). In addition, 10 extra frames with ulcer cases were used to train the f-SVM. We run our algorithm on those 50 frames, 20 ulcer frames, and 30 nonulcer frames, in order to estimate the sensitivity and specificity of our methodology.

Searching for other methodologies in the literature that might deal with the detection of ulcers in WCE videos, we found one work exclusively for ulcer detection [15]. As in [31], the authors use curvelet transform to extract the DCT coefficients. Using local binary pattern (LBP) and the DCT coefficients, texture descriptors are produced for the ulcers. Finally, a traditional MLP neural network is used to classify LBP inputs.

A comparison with other research works on the same dataset is not feasible due to inexistence of a public capsule endoscopy dataset.

Our methodology has focused on perforated ulcers since these are characteristic ulcers [16], whereas the authors of [15] do not clarify the type of ulcers they detect (see Table VI). There is a big difference in the patterns of various types of ulcers.

In both cases, detection of ulcers and detection of polyps, the difference and the novelty, if you will, of our proposed methodology compared to other works were taking into consideration the anatomical characteristics of these two types of abnormalities. Instead of having a traditional approach in which color and texture features are input to a trained neural network, we think that geometry features can play an important role in the detection scheme because this is how the physicals perceive and understand digestive tract structures.

VII. CONCLUSION AND DISCUSSION

In this paper, a novel synergistic methodology was proposed that deals with the detection of polyps and small bowel ulcers (perforated). More specifically, our proposed methodology is based on the robust and promising log Gabor filters, which behave successfully as a segmentation scheme. With log Gabor filters we managed to extract the dominating texture segments and leave out the background "less meaningful" textures, which is the goal of finding polyp candidates in WCE images. The SUSAN edge detector, as shown here, provides details for the

boundaries, of the regions, while the geometric characteristics like curvature and eccentricity produce the final polyp candidates. However, it should be mentioned that the use of SUSAN edge detector, and the calculation of curvature centers, add to the complexity of the methodology, making it impossible to be used in real time. A hardware implementation of the methodology could of course improve performance and perhaps make the methodology run real time. Further research on this direction has to be carried out.

The relatively low specificity shown in Table I derives from the fact that crisp regions exist in many WCE frames, which can be easily mistaken for polyp candidates. However, it can be argued that it is up to the gastroenterologist to decide whether a polyp candidate is truly a real polyp or just a normal crisp region of the intestine. But even with this strong argument, it is our responsibility to further reduce the false positives.

Regarding the detection of ulcers, again the log Gabor filters proved very beneficial to work as presegmentation step and create a mask for the segmentation process using the FRS algorithm (see Section V-B). In future, we plan to expand our methodology to include narrowing ulcer detection. For this direction, we used fuzzy SVMs which enable robust multiple class classification (perforated ulcers and narrowing ulcers) [30]. At the given moment, our classifier is only a two-class: perforated ulcer or not.

We considered using other features for describing ulcer patterns. These features were roundness and eccentricity. However, we ran several tests and they proved not to increase accuracy. This is probably due to the irregularity of the shape of each ulcer. There is not a standard shape for all ulcers (i.e., round or elongated) and such features cannot help as they do in the case of polyps. This conclusion might point out that more emphasis should be given on the color and texture techniques than geometry characteristics in the case of ulcers with irregular edges.

In both cases, detection of polyps and/or ulcers, the algorithm is scale and rotation invariant since it depends only on color and relative geometry characteristics. In that sense the methodology can operate on different aspect ratios of abnormal patterns. However, in reality since the resolution of the WCE video is quite small the algorithm can efficiently detect abnormalities of larger than 50 by 50 pixels on average.

As explained more thoroughly in our proposed video interpolation scheme [36], the capsule traverses through the digestive tract at various speeds, and some parts of the video can have high spatial resolution (multiple frames of a given structure) or poor resolution. Therefore, the polyps and ulcer detection scheme could be coupled with our interpolation scheme to increase the success rate in the case of different transit times.

Another limitation of the current scheme is that it does not take into consideration the presence of food substances or excessive mucus. Although this is not common this can create mostly false positives and reduce specificity.

We plan to create an even larger dataset including other pathological patterns such as blood-based abnormalities. Additionally, we want to expand the feature space to include time (frame number in the case of WCE videos) to add time as additional information.

ACKNOWLEDGMENT

The authors would like to thank Dr. M. Pouagare and Dr. O. Karargyris for their valuable contributions to this paper [35].

REFERENCES

[1] M. Yu, "M2 A capsule endoscopy. A breakthrough diagnostic tool for small intestine imaging," *Gastroenterol. Nurs.*, vol. 25, pp. 24–27, 2002.

[2] What I need to know about Colon Polyps? National Institute of Diabetes and Digestive and Kidney Diseases, National Institutes of Health. (Nov. 2008). [Online]. Available: http://digestive.niddk.nih.gov/ddiseases/pubs/colonpolyps_ez/

[3] S. A. Karkanis, D. K. Iakovidis, D. E. Maroulis, D. A. Karras, and M. Tzivras, "Computer aided tumor detection in endoscopic video using color wavelet features," *IEEE Trans. Inform Technol. Biomed.*, vol. 7, no. 3, pp. 141–152, Sep. 2003.

[4] L. A. Alexandre, N. Nobre, and J. Casteleiro, "Color and position versus texture features for endoscopic polyp detection," in *Proc. Int. Conf. Biomed. Eng. Informat.*, 2008, vol. 2, pp. 38–42.

[5] D. Chen, A. A. Farag, M. S. Hassouna, R. Falk, and G. W. Dryden, "Geometric features based framework for colonic polyp detection using a new color coding scheme," in *Proc. IEEE Int. Conf. Image Process.*, Sep. 16, 2007–Oct. 19, 2007, vol. 5, pp. V-17–V-20.

[6] J. Yao, M. Miller, M. Franaszek, and R. M. Summers, "Colonic polyp segmentation in CT colonography-based on fuzzy clustering and deformable models," *IEEE Trans. Med. Imag.*, vol. 23, no. 11, pp. 1344–1352, Nov. 2004.

[7] E. Konukoglu, B. Acar, D. S. Paik, C. F. Beaulieu, J. Rosenberg, and S. Napel, "Polyp enhancing level set evolution of colon wall: Method and pilot study," *IEEE Trans. Med. Imag.*, vol. 26, no. 12, pp. 1649–1656, Dec. 2007.

[8] A. K. Jerebko, S. Teerlink, M. Franaszek, and R. M. Summers, "Polyp segmentation method for CT colonography computer-aided detection," in *Proc. SPIE*, vol. 5031, pp. 359–369, May 2003.

[9] L. Zhao, C. P. Botha, J. O. Bescos, R. Truyen, F. M. Vos, and F. H. Post, "Lines of curvature for polyp detection in virtual colonoscopy," *IEEE Trans. Vis. Comput. Graph.*, vol. 12, no. 5, pp. 885–892, Sep./Oct. 2006.

[10] *Peptic Ulcers*, Harvard Medical School, Well-Connected Reports, Sep. 2001.

[11] eMedicineHealth—Practical Guide to Health. (Jan. 2009). http://www.emedicinehealth.com/peptic_ulcers/article_em.htm

[12] P. Y. Lau and P. L. Correia, "Detection of bleeding patterns in WCE video using multiple features," in *Proc. Int. Conf. IEEE Eng. Med. Biol. Soc.*, Lyon, France, Aug. 2007, pp. 5601–5604.

[13] A. Karargyris and N. Bourbakis, "Wireless capsule endoscopy and endoscopic imaging: A survey on various methodologies presented," *IEEE Eng. Med. Biol. Mag.*, vol. 29, no. 1, pp. 72–83, Jan./Feb. 2010.

[14] A. Karargyris and N. Bourbakis, "A methodology for detecting blood-based abnormalities in wireless capsule endoscopy videos," in *Proc. 8th IEEE Int. Conf. BioInf. BioEng.*, Oct. 8–10, 2008, pp. 1–6.

[15] B. Li and M. Q.-H. Meng, "Ulcer recognition in capsule endoscopy images by texture features," in *Proc. 7th World Congr. Intell. Control Autom.*, Jun. 25–27, 2008, pp. 234–239.

[16] U. S. Karnam, C. M. Rosen, and J. B. Raskin, "Small bowel ulcers," *Curr. Treat. Options Gastroenterol. J.*, vol. 4, no. 1, pp. 15–21, Feb. 2001.

[17] J. Daugman, "Uncertainty relation for resolution in space, spatial frequency and orientation optimized by two dimensional visual cortical filters," *J. Opt. Soc. Amer.*, vol. 2, no. 7, pp. 1160–1169, 1985.

[18] M. A. Webster and R. L. De Valois, "Relationship between spatial-frequency and orientation tuning of striate-cortex cells," *J. Opt. Soc. Amer. A*, vol. 2, pp. 1124–1132, 1985.

[19] What Are Log Gabor Filters and Why Are They Good? (Dec. 2008). [Online]. Available: http://www.csse.uwa.edu.au/∼pk/Research/MatlabFns/PhaseCongruency/Docs/convexpl.html

[20] D. Field, "Relations between the statistics of natural images and the response properties of cortical cells," *J. Opt. Soc. Amer.*, vol. 4, no. 12, pp. 2379–2394, 1987.

[21] S. M. Smith, "SUSAN—A new approach to low level image processing," Internal, Defence Research Agency, Surrey, U.K., Tech. Rep. TR95SMS1 1995.

[22] T. F. Chan and L. A. Vese, "Active contours without edges," *IEEE Trans. Image Process*, vol. 10, no. 2, pp. 266–277, Feb. 2001.

[23] M. Tkalcic and J. F. Tasic, "Colour spaces: Perceptual, historical and applicational background," in *Proc. IEEE Region 8 Comput. as Tool. EUROCON*, Sep. 22–24, 2003, vol. 1, pp. 304–308.
[24] Y. Ohta, T. Kanade, and T. Sakai, "Color information for region segmentation," *Comput. Graph. Image Process.*, vol. 13, no. 3, pp. 222–241, Jul. 1980.
[25] A. Moghaddamzadeh and N. Bourbakis, "A fuzzy technique for image segmentation of color images," in *Proc. 3rd IEEE Conf. Fuzzy Syst. IEEE World Congr. Comput. Intell.*, Jun. 26–29, 1994, vol. 1, pp. 83–88.
[26] V. N. Vapnik, *Statistical Learning Theory*. Hoboken, NJ: Wiley-Interscience, 1989.
[27] V. S. Kodogiannis and M. Boulougoura, "An adaptive neurofuzzy approach for the diagnosis in wireless capsule endoscopy imaging," *Int. J. Inform. Technol.*, vol. 13, no. 1, pp. 46–56, 2007.
[28] D. J. C. Barbosa, J. Ramos, J. H. Correia, and C. S. Lima, "Automatic detection of small bowel tumors in capsule endoscopy based on color curvelet covariance statistical texture descriptors," in *Proc. Annu. Int. Conf. IEEE Eng. Med. Biol. Soc.*, Sep. 3–6, 2009, pp. 6683–6686.
[29] R. M. Haralick, K. Shanmugam, and I. Dinstein, "Textural features for image classification," *IEEE Trans. Syst., Man, Cybern.*, vol. SMC 3, no. 6, pp. 610–621, Nov. 1973.
[30] T. Inoue and S. Abe, "Fuzzy support vector machines for pattern classification," in *Proc. Int. Joint Conf. Neural Netw.*, 2001, vol. 2, pp. 1449–1454.
[31] B. Li and M. Q.-H. Meng, "Computer-aided detection of bleeding regions for capsule endoscopy images," *IEEE Trans. Biomed. Eng.*, vol. 56, no. 4, pp. 1032–1039, Apr. 2009.
[32] R. Sidhu, D. S. Sanders, K. Kapur, L. Marshall, D. P. Hurlstone, and M. E. McAlindon, "Capsuleendoscopy: Is there a role for nurses as physician extenders?" *Gastroenterol. Nurs*, vol. 30, no. 1, pp. 45–48, Jan./Feb. 2007.
[33] F. Riaz, M. Dinis-Ribeiro, and M. Coimbra, "A review of current computer aided diagnosis systems for polyp detection in virtual colonoscopy," presented at the 7th Conf. Telecommunications, Santa Maria da Feira, Portugal, May 2009.
[34] M. Coimbra and J. P. Silva Cunha, "MPEG-7 visual descriptors—Contributions for automated feature extraction in capsule endoscopy," *IEEE Trans. Circuits Syst. Video Technol.*, vol. 16, no. 5, pp. 628–637, May 2006.
[35] Digestive Specialists, Inc., Dayton, OH.
[36] A. Karargyris and N. Bourbakis, "Three-dimensional reconstruction of the digestive wall in capsule endoscopy videos using elastic video interpolation," *IEEE Trans. Med. Imag*, vol. 30, no. 4, pp. 957–971, Apr. 2011.

Alexandros Karargyris received the Master's degree in electrical engineering and computer engineering from the National Technological University of Athens, Athens, Greece, in 2006. He received the Ph.D. degree in computer engineering from Wright State University, Dayton, OH, in 2010.

He is interested in computer vision and medical imaging analysis. He is a holder of NSF and Ohio Board of Regents (OBR) scholarships. He is currently a Research Fellow at the National Library of Medicine (NLM) of National Institutes of Health (NIH) Bethesda, MD. His current research includes the development of computer-aided detection algorithms for improving the usability and reducing process time of wireless capsule endoscopy videos.

Nikolaos Bourbakis (F'96) received the Ph.D. degree in computer science and computer engineering from the University of Patras, Rio, Greece.

He is currently an OBR Distinguished Professor of information technology, a Professor (j.a.) in Geriatrics in the School of Medicine, and the Director of the Assistive Technology Research Center, Wright State University, interfacing academia, industry, and government. He is publisher of more than 340 publications. His research interests include computer vision, image understanding, natural language text, artificial intelligence, information security, and assistive technologies research funded by government and industry.

Dr. Bourbakis is an editorial board member for several IEEE and international journals. He is the founder and the VP for the AIIS Inc. He is a recipient of several prestigious IEEE Awards.